A Phenomenological Model of Twinning-Mediated Strain Hardening

Alexei Vinogradov[1], Einar Agletdinov[2], Igor S. Yasnikov[2], Kristian Mathis[3] and Yuri Estrin[4,5]

[1]Department of Industrial and Mechanical Engineering, Norwegian University of Science and Technology - NTNU, 7491 Trondheim, Norway

[2]Institute of Advanced Technologies, Togliatti State University, Togliatti, 445667, Russia

[3] Department of Physics of Materials, Charles University, 12116, Prague, Czech Republic

[4]Department of Materials Science and Engineering, Monash University, Clayton, Victoria, 3800, Australia

[5]Drpartment of Mechanical Engineering. The University of Western Australia, Crawley WA 6009, Australia

Abstract

We present a model of strain-hardening in materials with twinning-mediated plasticity. While the model is largely phenomenological, it was motivated by microstructural considerations and can be claimed to be physically sound. Using simple, yet sensible, assumptions regarding the stress-driven twinning kinetics and dislocation-twin interactions, constitutive equations governing the strain hardening behaviour were obtained and solved numerically. The solutions were compared with the experimental data on uniaxial deformation of pure magnesium and Mg alloy ZK60, and this comparison substantiated the validity and practicality of the model proposed.

Keywords. Magnesium; twinning; phenomenological modelling; strain hardening; dislocation-twin interaction

1. Motivation and Background

The strain hardening behaviour of pure face-centred cubic (FCC) and body-centred cubic (BCC) metals is governed by the kinetics of dislocation slip, which is generally accepted and well-understood [1]. With the development of new structural materials whose microstructural evolution and the mechanical response are governed or affected by deformation twinning, understanding of the kinetics of this process and its interaction with lattice dislocations becomes crucial [2, 3]. In particular, comprehensive work has been highlighting the role of twinning in high strength austenitic steels with TWIP (TWinning Induced Plasticity) [4, 5], nanostructured materials [6-8], titanium [9], as well as magnesium and its alloys [10]. Common to all these materials is the preponderance of twinning that can be regarded as a key mechanism affecting nearly all aspects of their mechanical behaviour. Specifically, for Mg and its alloys having a hexagonal close-packed (HCP) structure, the strain hardening behaviour exhibits remarkable features, including a concave shape of the stress-strain curve and a pronounced asymmetry of the yield strength with respect to tension/compression, which are attributable to twinning [11-15]. Unlike the dislocation slip-controlled plasticity, which is understood in great detail, the role of twinning and its kinetics in the strain hardening process in low stacking fault energy FCC and HCP metals and alloys has been rationalised to a much lesser extent. This is particularly true for the description of twin accumulation in the course of deformation. Bouaziz and Guelton [16] suggested that the volume fraction of twins F in high manganese TWIP steels can be derived using the first-order kinetics assumption similar to that made by Olson and Cohen [17] for the martensitic transformation. In that approach, F as a function of strain ε takes the form $F = 1 - \exp(-m\varepsilon)$, where m is a parameter that depends on the stacking fault energy. This way of expressing the evolution of the twin volume fraction is very simple and

convenient, and it captures the exponential trend to saturation in a general manner. However, the approach itself is to be applied with care. First and foremost, there are reasons to believe that the twinning kinetics is stress-driven, rather than strain-driven [18-20]. This type of kinetics is obviously not covered by empirical relations of the $F = F(\varepsilon)$ form, cf. [16, 21-23].

In the last decade, multiple theoretical approaches were applied to describe twinning and dislocation slip phenomena in different materials at various length scales [24]. Specifically for HCP metals and alloys, the atomistic calculations [25, 26] were employed to simulate the mechanisms of twin nucleation, growth and twin boundary–dislocation interactions at microscale. At macroscale, a variety of crystal-plasticity models have been developed with the focus on texture evolution and the related anisotropy of the mechanical response and strain hardening characteristics of Mg and its alloys during monotonic and cyclic deformation [27-38]. Among the theories of strain hardening of materials where twinning is an essential deformation mode, a recent model due to Sahoo et al. [39] stands out as an attempt to combine the two-phase character of twin-containing materials, the polycrystal plasticity aspects, and the semi-empirical hardening behaviour of the matrix grains in which deformation twins are embedded.

Despite these partial successes of modelling, there is still a need for physically sound, reliable, and computationally economical phenomenological models of strain hardening in materials with twinning-mediated plasticity. Therefore, the main purpose of this study was to develop a model that would satisfy the mentioned need and consider the *stress-driven* twinning kinetics as an essential element of the constitutive description. As an outcome of this work, we present a robust microstructure-motivated phenomenological model of strain hardening in materials exhibiting concurrent dislocation slip and twinning and validate it by experimental data available for magnesium.

2. The Model

Beyond the yield point, the total strain ε in a material is comprised by the elastic, ε_{el}, and plastic, ε_{pl}, components taken additively:

$$\varepsilon = \varepsilon_{el} + \varepsilon_{pl} \tag{1}$$

Conventional tension or compression tests are performed at the constant total strain rate $\dot{\varepsilon}$:

$$\dot{\varepsilon} = \dot{\varepsilon}_{el} + \dot{\varepsilon}_{pl} = const = \frac{\dot{\sigma}}{E} + \dot{\varepsilon}_{pl} = \frac{\dot{\sigma}}{E} + \dot{\varepsilon}^{D} + \dot{\varepsilon}^{T} \tag{2}$$

where σ is the flow stress and E is the Young's modulus. (Henceforth, a dot denotes a time derivative.) The plastic stain rate $\dot{\varepsilon}_{pl}$ in the deforming specimen is determined by the evolution of the dislocation and twinning subsystems with the corresponding plastic strain rates $\dot{\varepsilon}1$ and $\dot{\varepsilon}^{T}$. An increment of the plastic shear strain, $d\gamma_{pl}$, is taken as a weighted sum of two contributions: the one due to dislocation slip, $d\gamma^{D}$, and the other due to deformation twinning, $d\gamma^{T} = \gamma^{T} dF$. Here γ^{T} is the shear strain produced when a twin is formed and dF is an increment of the twin volume fraction F. This 'elementary' shear strain γ^{T} is constant for a given crystal structure and twin system. Accordingly, the plastic shear strain increment is expressed as

$$d\gamma_{pl} = (1-F)d\gamma^{D} + \gamma^{T} dF \tag{3}$$

Converting the shear strains to axial ones through the Taylor orientation factor M, and passing from differentials to derivatives, Eq. (3) can be rewritten as:

$$\dot{\varepsilon}_{pl} = (1-F)\dot{\varepsilon}_{u}^{D} + \gamma^{T} \frac{\dot{F}}{M^{T}} \tag{4}$$

where $\dot{\varepsilon}_{u}^{D}$ denotes the plastic strain rate in the untwinned regions. Accordingly, $\dot{\varepsilon}^{D} = (1-F)\dot{\varepsilon}_{u}^{D}$ holds. The texture-dependent orientation factor for the twinning subsystem is defined as $M^{T} = \left\langle \frac{1}{SF(\Phi)} \right\rangle$ [40] with SF denoting the Schmid factor for the corresponding twin

system. The angle brackets denote averaging over the Euler angle Φ between the c axis of an HCP crystal and the loading axis:

$$M^T = \int_0^{\pi/2} \frac{1}{SF(\Phi)} \psi(\Phi) d\Phi \tag{5}$$

with $\psi(\Phi)$ denoting the texture dependent distribution function of the Schmid factor SF over Φ (see [21] for details).

To avoid confusion, we would like to state that Eqs. (3) and (4) do not imply the use of any form of a rule of mixtures for strain in the matrix and the twinned material (the iso-stress Sachs approach). Neither does the model invoke an iso-work assumption of Ref.[39]. Rather, it represents the ansatz made in the seminal publication by Bouaziz and Guelton [16] for the plastic strain increment for the entire material, with no distinction being made between the untwinned matrix and the twinned material. Our analysis (not included in the present paper) shows that the contribution from extra terms that would enter Eq. (4) if the iso-stress approach were taken are negligible and can be disregarded safely.

By combining Eqs. (2) and (4) the total strain rate is expressed as:

$$\dot{\varepsilon} = \frac{\dot{\sigma}}{E} + (1-F)\dot{\varepsilon}_u^D + \gamma^T \frac{\dot{F}}{M^T} \tag{6}$$

The plastic strain rate associated with dislocation slip, $\dot{\varepsilon}_u^D$, can be naturally recovered from the time-proven Kocks-Mecking-Estrin (KME) dislocation kinetics approach whereby the details of dislocation accumulation and recovery are implemented explicitly in first-order differential equations describing the dislocation density evolution [41-43]. In this single internal variable formulation, the total dislocation density ρ, which is considered as the key intrinsic variable of state, evolves according to an ordinary first-order differential equation $\dot{\rho}(t) = \dot{\varepsilon}_u^D(t) g(\rho)$, in which both dislocation storage and dislocation recovery terms are encompassed in the $g(\rho)$

function. A second internal variable of our model is the twin volume fraction *F*, the evolution of which will be discussed below.

In this work, a modified version of the KME [44] dislocation kinetic equation is proposed with the aim to account for the dislocation-twin interaction:

$$\frac{d\rho}{dt} = \dot{\varepsilon}_u^D M \left(\frac{k_0}{b\Lambda} - k_2 \rho \right) - k_3 \rho \dot{F} \tag{7}$$

This equation includes a dislocation storage term determined by the dislocation mean free path Λ, a dynamic dislocation recovery term $k_2\rho$ governed by the second-order dislocation annihilation kinetics, and an extra recovery term proportional to the volume fraction of twins F, which arises due to dislocation-twin interaction. The coefficients k_0, k_2, k_3 are parameters controlling the rates of the corresponding reactions. The third term on the right-hand side of Eq. (7) constitutes the chief difference from the original KME version. This term accounts for the dynamic dislocation recovery due to the interaction of lattice dislocations with twin boundaries.

These interactions are quite complex, as suggested by experimental and theoretical studies conducted at different length scales - from atomic [45] and nano- [46] levels to micro- and macro-scales [1, 47, 48]. The computational work by Serra and Bacon [49, 50] who investigated the annihilation of a basal dislocation by a twin boundary and the activation of twinning dislocation sources deserves special mention. However, the dislocation-twin boundary processes, especially for the dynamic case involving twin boundary motion, are not fully understood. Just like ordinary grain boundaries, twin boundaries serve as sources and/or sinks of dislocations. Besides, twin boundaries obstruct the transmission of dislocations from one side of the twin boundary to the other [6], thus impeding dislocation motion and increasing the dislocation accumulation rate. One might thus expect that twin boundaries would give rise to increased dislocation density accumulation. This picture is not unequivocal, though, as dislocations can effectively transmit slip across twin boundaries by activation of dislocation

sources on the opposite side of a boundary [51-54]. Perhaps somewhat counter-intuitively, the general belief is that, on balance, the dislocation density is *reduced*, rather than increased, due to dislocation interactions with twin boundaries. Since the early work by Müllner and Solenthaler [55] it has been broadly recognised that deformation twinning significantly facilitates the dynamic dislocation recovery. As a result of the twin-stimulated recovery, the residual dislocation density is markedly lower if deformation twinning is active compared to that observed after pure dislocation slip-mediated deformation. This is supported by [56] where it was observed that profuse twinning in severely deformed Hadfield steel was accompanied with a *reduction* of the dislocation density. Thus, the contribution of deformation twinning to strain hardening is seen to be two-fold: (i) due to its influence on the dislocation density accumulation through the reduction of the dislocation mean free path, as reflected in the first term of Eq.(7), and (ii) due to an extra contribution to the dislocation annihilation rate represented by the third term in the equation.

Effects of latent twin hardening due to formation of sessile dislocations at the twin boundaries [52, 53] are not considered here. Besides, we do not distinguish between different dislocation slip systems and types of dislocations, thereby reducing a complex crystal plasticity problem to its simplified single internal variable version.

The Taylor relation

$$\sigma = \sigma_0 + \hat{\alpha} G b M \sqrt{\rho} \tag{8}$$

that links the flows stress to the total dislocation density involves the shear modulus G and the 'friction' stress σ_0; the factor $\hat{\alpha} = 0.1...0.5$ depends on, but is not very sensitive to the deformation mode [57], temperature, and strain rate [58]. The Taylor relation holds ubiquitously for virtually any dislocation configurations in deforming metals and alloys and is a pivotal ingredient of the dislocation-based plasticity theories. Using this relation, after simple

rearrangements in Eq.(7), we obtain an equation for the plastic strain rate associated with dislocation slip $\dot{\varepsilon}_u^D$ in the form:

$$\dot{\varepsilon}_u^D = \frac{2(\sigma-\sigma_0)\dot{\sigma}+k_3(\sigma-\sigma_0)^2\dot{F}}{\frac{k_0M(\hat{\alpha}GbM)^2}{b\Lambda}-k_2M(\sigma-\sigma_0)^2} \tag{9}$$

The dislocation mean free path Λ is determined by the preponderant obstacles to dislocation slip, of which the immobile (forest) dislocations stored in the grain interior and the grain boundaries are most commonly included in different versions of the KME equations. Since the twin boundaries act as strong obstacles to dislocation slip, the value of the dislocation mean free path can be obtained from [16, 23, 59]:

$$\frac{1}{\Lambda}=\frac{1}{D_m}+\frac{1}{t} \tag{10}$$

where D_m is the mean grain size and *t* is the mean inter-twin spacing which can be related to the mean twinning plate thickness *h* through Fullman's stereological equation [60, 61]

$$F=\frac{2h}{t+2h} \tag{11}$$

By eliminating *t* from Eqs. (10) and (11), the following expression for Λ is obtained:

$$\frac{1}{\Lambda}=\frac{1}{D_m}+\frac{F}{2h(1-F)} \tag{12}$$

By substituting Eq. (12) for $1/\Lambda$ in Eq. (9), one obtains an equation for the strain rate accommodated by dislocation slip:

$$\dot{\varepsilon}_u^D = \frac{2(\sigma-\sigma_0)\dot{\sigma}+k_3(\sigma-\sigma_0)^2\dot{F}}{k_0Mb(\hat{\alpha}GM)^2\left(\frac{1}{D_m}+\frac{F}{2h(1-F)}\right)-k_2M(\sigma-\sigma_0)^2} \tag{13}$$

By plugging Eq.(13) into Eq. (6) the equation for the total strain rate takes the following form:

$$\dot{\varepsilon}=\frac{\dot{\sigma}}{E}+\frac{\left(1-F\right)\left(2\dot{\sigma}+k_3\left(\sigma-\sigma_0\right)\dot{F}\right)}{\frac{k_0 Mb\left(\hat{\alpha}GM\right)^2}{\left(\sigma-\sigma_0\right)}\left(\frac{1}{D_m}+\frac{F}{2h\left(1-F\right)}\right)-k_2 M\left(\sigma-\sigma_0\right)}+\gamma^T\frac{\dot{F}}{M^T} \tag{14}$$

Solving the latter equation for σ requires an explicit form of the twin volume fraction as a function of time $F=F(t)$. Following the approach proposed in [20] for the stress-driven twinning kinetics, the following additional assumptions are made: (i) there exists a critical stress below which no twinning occurs; (ii) the stress required for twin nucleation is higher than that for twin propagation; (iii) under a stress exceeding the critical twin nucleation stress, a twin nucleates, propagates lengthwise through the grain and acquires a length *L*, which is of the order of the grain size *D* ($L\sim D$), as illustrated schematically in Fig. 1a and as is often observed in experiment [62, 63]. The results of direct video observations corroborating the proposed scenario are shown in Fig. 1b and in greater detail in Fig. 2. We note that this assumption works particularly well for polycrystals with relatively small grains [64]; (iv) the average thickness of the nucleated twin, h, is generally assumed to be independent of grain size or twin length following the arguments present in [65]; however, (v) if the generated twin of length *L* is in equilibrium, Friedel's formula relating the twin width to its length and the applied stress holds [66] (see also [67] and [19]):

$$\sigma=M^T\frac{G}{2}\gamma^T\frac{h}{L}\approx M^T\frac{G}{2}\gamma^T\frac{h}{D} \tag{15}$$

In the present work, we confine ourselves to the simplest approximation where we do not account for the twin-induced changes in the grain size distribution. Neither do we distinguish between the twins operating on different twinning systems. Note that, since the thickness of the freshly nucleated twin is small and is considered constant, dislocation slip in the twinned regions is not taken into account in the present version of the model. It can easily be included in future model extensions, though. As a matter of fact, the *in situ* optical microscopy evidence for magnesium suggests that under uniaxial compression, deformation

twins within a grain were formed on a single slip system starting from a coarse grain and progressing to finer and finer grains. This is demonstrated by a sequence of images in Fig. 2, which illustrates the key assumptions of the model regarding the twinning behaviour in polycrystalline Mg (see [63] for experimental details).

In terms of grain size, grains in polycrystalline aggregates are commonly distributed log-normally [68] with the probability density function given by:

$$f(D) = \frac{1}{D\sigma_D\sqrt{2\pi}} \exp\left(-\left(\frac{\ln(D/D_m)}{\sqrt{2}\sigma_D} \right)^2 \right) \tag{16}$$

where D_m is the mean grain size defined as $D_m = \int_{D_{\min}}^{D_{\max}} D f(D)\, dD$ and σ_D^2 is the variance of the distribution. The log-normal distribution is commonly observed as a result of random nucleation and growth processes, such as crystallisation or recrystallisation [69, 70], e.g. during magnesium fabrication.

The volume of a twin generated in a grain of size D will be proportional to $D^2 h$. The grains with a size in the interval from D to $D + dD$ will contribute a differential of the twin volume fraction dF given by

$$dF = \alpha \frac{hD^2}{D_m^3} f(D)\, dD \tag{17}$$

where $\alpha = \alpha_T \bar{N}_T$ is a model parameter that contains as a factor the fraction of grains capable of undergoing twinning and the average number of twins per grain $\bar{N}_T$. The coefficient α_T is texture dependent [65, 71], and it can be determined experimentally. According to [72], its value ranges from 0.3-0.5. In reality, the average number of twins per grain $\bar{N}_T$ depends on grain size [62, 65, 73, 74]: fewer twins are observed in smaller grains compared to grains of similar orientation but larger in size. Deformation twins appear as thin lenticular (HCP) or plate-like (FCC) reoriented layers bounded by near-parallel twin boundaries, Figs. 1 and 2. Capolungo

et al. [65] found *h* to be rather insensitive to grain size and orientation. Kumar et al. [75] noticed correctly that the widely reported grain size effects on the geometry of twins refer predominantly to late stages of twin growth, rather than to an early stage of twin nucleation where the twin thickness does not increase considerably, Figs. 1 and 2. This assertion was further exploited by Wu et al. [76] in developing a constitutive model of twin nucleation and propagation in magnesium.

It should also be noted that a recent statistical analysis of features of early twinning in polycrystalline titanium deformed to small strains (below 2%) did not reveal their sensitivity to grain size or grain orientation [77]. Rather, this early twinning was associated with incompatibility stresses between deforming neighbouring grains. The relevance of such effects to twinning in magnesium is yet to be investigated and, if appropriate, they can be included in the present model in a phenomenological way.

Using Friedel's formula, Eq. (15), and combining it with Eqs. (16) and (17), the twin volume fraction was obtained in [20] as a solution of the following differential equation:

$$\frac{dF}{dt}=\frac{\alpha h^3\left(M^T G\gamma^T\right)^2}{4\sqrt{2\pi}D_m^3\sigma_D}\frac{1}{\sigma^3}\frac{d\sigma}{dt}\theta\left(\sigma-\sigma_{cr}\right)\exp\left(-\frac{\ln^2\left(\frac{M^T G\gamma^T h}{2D_m\sigma}\cdot\theta\left(\sigma-\sigma_{cr}\right)\right)}{2\sigma_D^2}\right) \tag{18}$$

The Heaviside function $\theta\left(\sigma-\sigma_{cr}\right)$ is introduced to account for the critical stress σ_{cr} required for the onset of twinning. When this stress is reached during loading, all grains with the size greater than

$$D_c\cong\frac{M^T\gamma^T h}{2}\frac{G}{\sigma_c} \tag{19}$$

will undergo twinning. Thus, being footed on Eqs. (15)-(17), the model tacitly assumes that coarse grains yield first and as the stress increases beyond the twin initiation stress, smaller and smaller grains become engaged in the generation of twins. This was corroborated by direct

video observations [20] and the results of statistical analysis of $\{10\bar{1}2\}$ twin lamellae performed by Lou et al. [78] on a hot-rolled AZ31 alloy.

Equations (14) and (18) represent a complete set of equations describing the strain hardening behaviour, which accounts for the evolution of interacting dislocation and twin subsystems. This set of equations can be represented in a compact form as an autonomous non-linear set of first-order differential equations $\begin{cases} \dot{\sigma} = Z_1(\sigma; F) \\ \dot{F} = Z_2(\sigma; F) \end{cases}$, with $Z_i, (i = 1, 2)$ being transcendental functions whose explicit form is given in the Appendix.

3. Model verification

3.1. Verification method

To obtain the model parameters entering Eqs. (14) and (18), the model predictions were fitted to the experimental data by minimising the objective function defined as

$$f(\bar{p}) = \sum_{i=1}^{N} (\sigma(\bar{p})_i^{\text{model}} - \sigma_i^{\text{data}})^2 \tag{20}$$

Here $\sigma(\bar{p})_i^{\text{model}}$ is the stress vector obtained by solving the set of Eqs. (14) and (18) for a given set of parameters denoted symbolically as $\bar{p}$; σ_i^{data} is the stress vector obtained experimentally, and *N* is the number of readings in the stress vector. The input for the optimisation algorithm is the initial set of parameters $\bar{p}_0$. At each iteration, the parameters are varied within a pre-set range of permissible values. The model system is solved numerically with this set of parameters, and the solution is used to calculate the objective function. The iterations continue until the objective function, Eq. (20), is minimised.

For solving the set of equations (14) and (18) numerically, the LSODA/LSODE (Livermore Solver for Ordinary Differential Equations) method - a popular solver for initial value problems for sets of ordinary differential equations [79] - was employed. This procedure determines the

stiffness of the problem and applies different solvers to stiff and non-stiff systems. For stiff problems, the backward differentiation method is used. If the problem is not stiff, the Adams predictor-corrector method is applied.

In this study, two optimisation methods were employed to find the adjustable parameters k_0, k_1, k_3. The first method used was the AMPGO optimisation algorithm (Adaptive Memory Programming for Global Optimization [80]), which is a multi-start method based on adaptive memory programming, which involves memory structures that are superimposed on a local optimiser. The differential evolution (DE) method [81] we employed as well is another popular stochastic direct search technique which is widely used for optimisation. The DE algorithm optimises a problem by iteratively trying to improve a candidate solution with regard to a given measure of quality. The advantage of the DE strategy is that it makes few or no assumptions about the problem and can search very large spaces of candidate solutions. Interested readers are encouraged to refer to the above references for further details of the optimisation procedures, algorithms, and codes. Optimisation based on both methods used in the present work returned similar results.

3.2. Materials and testing

The capacity of the proposed approach for modelling strain hardening was tested on samples with different manufacturing histories and various grain size distributions, texture, and mechanical responses. Below, the results will be first demonstrated on several examples of tension and compression tested pure (99.95%) magnesium in the as-cast state, for which detailed microstructural results were reported earlier by some of the present authors in [82]. Here, the dislocation density as well as the volume fraction of twins were available from the neutron diffraction results reported in [82], which made this material an ideal candidate for model verification. Furthermore, the same specimen was also independently tested using the *in situ*

acoustic emission (AE) method (see [82] for detail). In brief, the AE data were acquired continuously in a thresholdless mode of operation with a 16 bits resolution at 2 Msamples/s rate. The dataset was processed following the non-supervised adaptive sequential *k*-means (ASK) clustering procedure developed in [83] to discriminate between contributions from different modes of plastic deformation. Specifically, twinning and dislocation slip on different systems can be distinguished by this method reliably [84, 85] and their kinetics can be followed separately or in parallel. The signals stemming from different sources are discriminated on the statistical basis using the normalised AE power spectral density as the input for comparison with the Kullback-Liebler distance as a measure of similarity/dissimilarity between AE spectra generated by different mechanisms, which are finally assigned to corresponding clusters. In addition, the experimental and the simulated stress-strain curves for Mg after hot extrusion at 350^{o}C with an extrusion ratio of 10:1 will be compared as a model validation exercise. Finally, the quality of the model prediction will also be demonstrated for a weakly textured annealed alloy ZK60 (Mg–5.8Zn–0.44Zr, in wt.%, see [84, 86] for details of the microstructure and mechanical properties).

To evaluate grain size distributions in all specimens tested, optical microscopy and electron back-scattered diffraction were employed. Typical examples of the binarised images showing the grain morphology in the specimens tested are shown in Fig. 3. For grain size measurements, the *ImageJ* software [87] was used in conjunction with the equivalent diameter method. Since the grains were nearly equiaxed, this method rendered almost the same result as the standard ASTM linear intercept method for the mean grain size. Corresponding grain size distributions are shown in Fig. 4, where the histograms represent the experimental data and the solid lines are obtained using the non-linear curve fitting by the log-normal function. One can see that the assumption of log-normal grain size distributions holds reasonably well for all specimens tested. The values of the parameters of these distributions are shown in Table 1.

These values were used in the model calculations. The elastic moduli *E* and *G* for Mg were taken as 44 and 16.3 GPa, respectively. The values of $\hat{\alpha}=0.3$, b=3.5×10^{-10} m, γ^{T} =0.129 and M=4.5 were kept constant in all calculations. Following Capolungo et al. [65], the average twin thickness *h* was initially set at 2 μm and then optimised to fit the experimental data. (We note that the variation of *h* in this optimisation exercise was not very large.) Other model parameters are also listed in Table 1.

3.3. Experimental results and comparison with the model

The model presented in the foregoing section reproduces the observed stress-strain response of all materials tested reasonably well, as illustrated in Figs. 5-7. An important feature is the ability of the model to capture the concave-upward trend in the stress-strain curves, which is commonly associated with twinning, and which is pronounced in magnesium to a certain extent depending on texture and grain size.

Figure 5 also compares the model predictions for the total dislocation density and the twin volume fraction with that estimated from neutron diffraction data for both tension and compression tests of pure Mg (specimen (a) in Figs.3 and 4). It is obvious that the model fits the data for the dislocation density well (within the experimental scatter of $\rho(\varepsilon)$ estimates by the neutron diffraction technique). The model performs less satisfactorily with regard to the second key internal variable, which underestimated by theoretical predictions. The reason is that the model in its present form, which assumes the constancy of *h* during deformation, does not account for twin growth commonly observed in magnesium and its alloys. It does predict the correct functional dependence $F\left(\varepsilon\right)$, though, and can, in principle, be further fine-tuned to experiments showing larger saturation values for the twin volume fraction. This would require a separate kinetic equation for twin thickening. We should like to emphasise that even without

such fine-tuning, the model shows good qualitative agreement with experimental results. It should also be noted that the model is in better agreement with the $F(\varepsilon)$ data for tension than compression. As was shown in [72, 82], the evolution of twinning in randomly oriented Mg polycrystals is markedly different in these two cases. When a tensile load is applied, the number of nucleated twin variants within a single grain increases with the increasing Schmid factor (SF^T) for extension twinning. For an ideally oriented grain (SF^T=0.5) all six possible twin variants can be observed, which mutually hinder twin growth. Furthermore, twinning can occur in grains with very low SF^T as well [72]. By contrast, in the case of compression, only one or two variants nucleate in suitably oriented grains, and these twins can thicken readily. There is a threshold value for the deviation of the crystallographic *c*-axis from the loading direction (46°51'), above which no twinning occurs in compression [88]. Finally, the overall fraction of the "twinning-oriented" grains (SF^T> 0.3) is much higher in compression (~ 40% vs. ~20% in tension). This means that in tension there is a greater number of nucleated twins. A higher twin volume fraction observed in compression can be attributed to twin thickening – a process which is not captured by the present model.

The remarkable agreement between the ASK-powered AE-based assessment of the kinetics of dislocation slip and deformation twinning and the model predictions is particularly noteworthy. This is illustrated in Figs. 5b and 7 for polycrystalline as-cast Mg (specimen (a) in Figs. 3 and 4). Dislocation slip and deformation twinning generate AE signals with markedly different waveform features, and their relative contributions evolve during deformation in distinctly different ways. Salient differences between these two mechanisms are commonly associated with the shapes of the AE waveforms and the amplitude and power of the AE signals (low amplitude/low power AE with a broad spectrum and pronounced low-frequency component for dislocation slip as opposed to high amplitude/high power AE with a predominant high frequency component in the spectral density for twinning). It should be

noted that AE is capable to detect only the stage of twin nucleation and propagation (i.e. the length-wise growth) [89]. Since the twin thickening is a substantially (orders of magnitude) slower process than nucleation [90], it is below the detection limit of the AE method. This means that the twin-induced AE is directly related to the number and the length of the nucleated twins [90]. Thus, with appropriate calibration, the kinetics of the evolution of the twin volume fraction can be recovered by means of AE using the cumulative AE power (or energy) as a parameter proportional to the transformed (twinned) volume [85]. Direct video observations [91] and more precise data of SEM EBSD [92] and neutron diffraction [72, 93] show that twin accumulation follows a sigmoidal curve with a trend to saturate, which is in fair agreement with the integral AE measurements and the model predictions of the current work, Fig. 5.

To get a better insight in the model's performance, it is instructive to observe the behaviour of the strain rate components $\dot{\varepsilon}^D$ and $\dot{\varepsilon}^T$ as functions of strain individually. These components were calculated using Eq. (9) and associating $\dot{\varepsilon}^T$ with the second term on the right-hand side of Eq.(4) ($c = \gamma^T \dot{F} / M^T$), respectively. Results are shown in Fig. 6 (a), where the model predictions are presented vis-à-vis the relative (normalised) AE activity assessed separately for dislocation slip and twinning. Figure 6 (b) provides further details based on a juxtaposition of AE and neutron diffraction data [82] and making a distinction between the different AE classes, including those associated with basal slip, non-basal slip, and twinning. It is seen that the model predicts that at the onset of plastic flow, the dislocation slip dominates, the corresponding rate of plastic deformation increases, reaches its maximum and then drops off when twinning is activated and the strain rate it contributes becomes considerable. Apparently, both mechanisms operate concurrently throughout the test. However, it is the twinning activity that is responsible for the concavity of the stress-strain curve, which occurs at the same time as a maximum in $\dot{\varepsilon}^T$. It is remarkable that AE reflecting the activity of both deformation modes behaves in very much the

same manner as the corresponding strain rates, Fig. 6a. The commonly observed fact that AE detects considerable twinning from the very beginning of deformation contradicts the model prediction of a low overall contribution of twinning at the early deformation stages. One should bear in mind, however, that AE is extremely sensitive to twinning so that even a very fine individual twin is detectable by AE. Therefore, despite the values of $\dot{\varepsilon}^T$ being quite small, twinning-induced AE is detected. This AE component increases and then diminishes in parallel with $\dot{\varepsilon}^T$ in excellent agreement with the model predictions. Similarly, although in a mirror-like manner, the dislocation-related AE component exhibits a minimum when the $\dot{\varepsilon}^D$ value is lowest and $\dot{\varepsilon}^T$ is highest.

Finally, it is of interest to discuss the role of the last term on the right-hand side of Eq.(7), which refers to the rate of dislocation density reduction due to the interaction of dislocations with growing twins. When dislocations are 'harvested' by a growing twin, the kinetics of their density evolution is controlled by the rate of twin volume fraction accumulation (time derivative *dF/dt*) and the magnitude of the rate parameter k_3. A family of model stress-strain curves with different k_3 values was simulated for a given $F(t)$, as shown in Fig. 8. One can notice that an increase in the k_3 value reduces the strain hardening rate and gradually "straightens" the concavity of the stress-strain curves, which is particularly pronounced in the strain range where the twin volume fraction changes most rapidly. The strikingly different stress-strain response of pure Mg in tension and compression suggests that the contribution of the different mechanisms to the overall strain hardening has strong directionality. In line with the discussion given in Section 3.3, this accounts for the variability of the values of the parameters k_1, k_2, and k_3 listed in Table 1.

4. Conclusions

The main thrust of the present paper is on the strain hardening mechanisms and the role of the interplay between the dislocation slip and mechanical twinning in the deformation behaviour of materials with twinning-mediated plasticity. We presented a microstructurally-motivated phenomenological model of strain hardening tuned for magnesium and its alloys, although, in principle, it can be adapted for other materials prone to deformation twinning. The stress-driven nature of grain size dependent mechanical twinning is central to the model. The general frame of the model is provided by the two internal variables approach, with the total dislocation density and the twin volume fraction as intrinsic variables evolving in the process of straining. Using simple, yet sensible, assumptions regarding the stress-driven twinning kinetics and dislocation-twin interactions, constitutive equations governing the strain hardening behaviour were obtained and solved numerically. The solutions were compared with the experimental stress-strain curves for pure Mg and the Mg alloy ZK60. The evolution of the twin volume fraction and the dislocation density during uniaxial loading was assessed independently by the acoustic emission and neutron diffraction methods *in situ*. Very good agreement between experimental observations and model predictions was found, thus supporting the general approach and the specific assumptions made. Despite its simplicity, the model recovers the mechanical behaviour of Mg and its alloys faithfully. Quite importantly, it accounts for a characteristic concave shape of the deformation curves caused by the twinning activity. It also reflects the complexity of interplay between the two major deformation modes that results in characteristically different deformation stages corresponding to the different activity of the underlying deformation mechanisms.

CRediT author statement

Alexei Vinogradov: Conceptualization, Methodology, Original draft preparation, Supervision. Einar Agletdinov: Data curation, Software, Formal analysis, Validation. Igor Yasnikov: Investigation. Krstian Mathis: Investigation. Yuri Estrin: Methodology, Writing- Reviewing and Editing.

Acknowledgements

The support from the Ministry of Education and Science of RF through the State Assignment according to the contract No. 11.5281.2017/8.9 is gratefully appreciated. KM is thankful for the support of the Czech Science Foundation through the grant No. 18-07140S. Two of the authors (AV and YE) would like to acknowledge useful discussions with Prof. Horst Biermann, Dr. Stefan Martin and Dr. Anja Weidner of CRC 799, TU Bergakademie Freiberg, Germany. Their insights in the deformation twinning phenomena in steels have been of great value for developing the present modelling frame for twinning in magnesium.

Data availability.

The experimental data that support the findings of this study are available from the corresponding author, AV, upon reasonable request.

Appendix.

The explicit form of the set of constitutive equations is represented as:

$$\begin{cases} \dot{\sigma} = \dfrac{\dot{\varepsilon}}{\dfrac{1}{E} + \dfrac{2(1-F)}{\dfrac{k_0 Mb(\hat{\alpha}GM)^2}{(\sigma-\sigma_0)}\left(\dfrac{1}{D_m}+\dfrac{F}{2h(1-F)}\right) - k_2 M(\sigma-\sigma_0)} + \left(\dfrac{k_3(\sigma-\sigma_0)}{\dfrac{k_0 Mb(\hat{\alpha}GM)^2}{(\sigma-\sigma_0)}\left(\dfrac{1}{D_m}+\dfrac{F}{2h(1-F)}\right) - k_2 M(\sigma-\sigma_0)} + \dfrac{\gamma^T}{M^T}\right)\dfrac{\zeta}{\gamma^T}\left(\dfrac{\xi}{\sigma}\right)^3 \exp\left(-\dfrac{\ln^2\left(\dfrac{\xi\theta(\sigma-\sigma_{cr})}{2\sigma}\right)}{2\sigma_D^2}\right)} \\ \dot{F} = \dfrac{\dot{\varepsilon}\dfrac{\zeta}{\gamma^T}\left(\dfrac{\xi}{\sigma}\right)^3 \exp\left(-\dfrac{\ln^2\left(\dfrac{\xi\theta(\sigma-\sigma_{cr})}{2\sigma}\right)}{2\sigma_D^2}\right)}{\dfrac{1}{E} + \dfrac{2(1-F)}{\dfrac{k_0 Mb(\hat{\alpha}GM)^2}{(\sigma-\sigma_0)}\left(\dfrac{1}{D_m}+\dfrac{F}{2h(1-F)}\right) - k_2 M(\sigma-\sigma_0)} + \left(\dfrac{k_3(\sigma-\sigma_0)}{\dfrac{k_0 Mb(\hat{\alpha}GM)^2}{(\sigma-\sigma_0)}\left(\dfrac{1}{D_m}+\dfrac{F}{2h(1-F)}\right) - k_2 M(\sigma-\sigma_0)} + \dfrac{\gamma^T}{M^T}\right)\dfrac{\zeta}{\gamma^T}\left(\dfrac{\xi}{\sigma}\right)^3 \exp\left(-\dfrac{\ln^2\left(\dfrac{\xi\theta(\sigma-\sigma_{cr})}{2\sigma}\right)}{2\sigma_D^2}\right)} \end{cases}$$

where $\xi = \dfrac{M^T G\gamma^T h}{D_m}$ and $\zeta = \dfrac{\alpha\theta(\sigma-\sigma_{cr})}{4\sqrt{2\pi}\sigma_D M^T G}$.

Table 1. Parameters used in calculations

Parameter	Sample				
	Mg (as-cast) fine grain compression	**Mg (as-cast) fine grain tension**	**Mg (as cast) coarse grain**	**Mg (extruded)**	**ZK60**
Grain structure	Fig. 3a	Fig. 3a	Fig. 3b	Fig. 3c	Fig. 3d
Grain size distribution	Fig. 4a	Fig. 4a	Fig. 4b	Fig. 4c	Fig. 4 d
Stress-strain curve	Fig. 4b	Fig. 4a	Fig. 7a	Fig. 7b	Fig. 7c
σ_0, MPa	3	0.7	2.3	3.5	10
h, μm	2.5	3.7	5	1.9	0.6
M^T	2.5	2.3	2.5	2.2	2.23
k_0	44	810	2	53	542
k_2	1	251	50	1.9	59
k_3, m^{-2}	10	650	100	77	5
D_m, μm	95	88	500	54	82
σ_D	0.19	0.5	1.07	0.39	0.20
α	2.71	1.90	3.9	3.65	3.04
&, s^{-1}	$1x10^{-3}$	$1x10^{-3}$	$8.4x10^{-4}$	$1.7x10^{-4}$	$7x10^{-4}$
σ_{cr}, MPa	3	12	0.02	5	96

References

[1] J.W. Christian, S. Mahajan, Deformation twinning, Progress in Materials Science 39(1–2) (1995) 1-157.
[2] L. Lu, Y. Shen, X. Chen, L. Qian, K. Lu, Ultrahigh Strength and High Electrical Conductivity in Copper, Science 304(5669) (2004) 422-426.
[3] X.L. Wu, Y.T. Zhu, Inverse Grain-Size Effect on Twinning in Nanocrystalline Ni, Physical Review Letters 101(2) (2008) 025503.
[4] G. Frommeyer, U. Brux, P. Neumann, Supra-Ductile and High-Strength Manganese-TRIP/TWIP Steels for High Energy Absorption Purposes, ISIJ International 43(3) (2003) 438-446.
[5] B.C. De Cooman, Y. Estrin, S.K. Kim, Twinning-induced plasticity (TWIP) steels, Acta Materialia 142 (2018) 283-362.
[6] K. Lu, L. Lu, S. Suresh, Strengthening Materials by Engineering Coherent Internal Boundaries at the Nanoscale, Science 324(5925) (2009) 349-352.
[7] Y. Li, Y.H. Zhao, W. Liu, C. Xu, Z. Horita, X.Z. Liao, Y.T. Zhu, T.G. Langdon, E.J. Lavernia, Influence of grain size on the density of deformation twins in Cu–30%Zn alloy, Materials Science and Engineering: A 527(16–17) (2010) 3942-3948.
[8] Y.T. Zhu, X.Z. Liao, X.L. Wu, Deformation twinning in nanocrystalline materials, Progress in Materials Science 57(1) (2012) 1-62.
[9] A.A. Salem, S.R. Kalidindi, R.D. Doherty, Strain hardening of titanium: role of deformation twinning, Acta Materialia 51(14) (2003) 4225-4237.
[10] C. Bettles, M. Barnett, Advances in wrought magnesium alloys: Fundamentals of processing, properties and applications, Woodhead Publishing Ltd., Philadelphia, USA, 2012.
[11] M.R. Barnett, Twinning and the ductility of magnesium alloys. Part I: "Tension" twins, Materials Science and Engineering A 464(1-2) (2007) 1-7.
[12] M.R. Barnett, Twinning and the ductility of magnesium alloys. Part II. "Contraction" twins, Materials Science and Engineering A 464(1-2) (2007) 8-16.
[13] S.R. Agnew, Deformation mechanisms of magnesium alloys, in: C. Bettles, M. Barnett (Eds.), Advances in Wrought Magnesium Alloys: Fundamentals of Processing, Properties and Applications, 2012, pp. 63-104.
[14] K. Máthis, F. Chmelík, M. Janeček, B. Hadzima, Z. Trojanová, P. Lukáč, Investigating deformation processes in AM60 magnesium alloy using the acoustic emission technique, Acta Materialia 54(20) (2006) 5361-5366.
[15] B.C. Suh, M.S. Shim, K.S. Shin, N.J. Kim, Current issues in magnesium sheet alloys: Where do we go from here?, Scripta Materialia 84-85 (2014) 1-6.
[16] O. Bouaziz, N. Guelton, Modelling of TWIP effect on work-hardening, Materials Science and Engineering: A 319–321(0) (2001) 246-249.
[17] G.B. Olson, M. Cohen, Kinetics of strain-induced martensitic nucleation, Metallurgical Transactions A 6(4) (1975) 791-795.
[18] Y.F. Shen, N. Jia, Y.D. Wang, X. Sun, L. Zuo, D. Raabe, Suppression of twinning and phase transformation in an ultrafine grained 2 GPa strong metastable austenitic steel: Experiment and simulation, Acta Materialia 97 (2015) 305-315.
[19] J.T. Lloyd, A dislocation-based model for twin growth within and across grains, Proceedings. Mathematical, physical, and engineering sciences 474 (2018) 20170709-20170709.
[20] A. Vinogradov, E. Vasilev, D. Merson, Y. Estrin, A phenomenological model of twinning kinetics, Advanced Engineering Materials 19(1) (2017) 1600092.
[21] M.R. Barnett, Texture, twinning and uniform elongation of wrought magnesium, Materials Science Forum, 2005, pp. 1079-1084.
[22] O. Bouaziz, S. Allain, C. Scott, Effect of grain and twin boundaries on the hardening mechanisms of twinning-induced plasticity steels, Scripta Materialia 58(6) (2008) 484-487.
[23] O. Bouaziz, Strain-hardening of twinning-induced plasticity steels, Scripta Materialia 66(12) (2012) 982-985.

[24] H. Abdolvand, M.R. Daymond, Multi-scale modeling and experimental study of twin inception and propagation in hexagonal close-packed materials using a crystal plasticity finite element approach—Part I: Average behavior, Journal of the Mechanics and Physics of Solids 61(3) (2013) 783-802.
[25] A. Serra, R.C. Pond, D.J. Bacon, Computer-Simulation of the Structure and Mobility of Twinning Dislocations in Hcp Metals, Acta Metallurgica et Materialia 39(7) (1991) 1469-1480.
[26] C. Tomé, I. Beyerlein, J. Wang, R. McCabe, A multi-scale statistical study of twinning in magnesium, JOM 63(3) (2011) 19-23.
[27] T. Mayama, K. Aizawa, Y. Tadano, M. Kuroda, Influence of twinning deformation and lattice rotation on strength differential effect in polycrystalline pure magnesium with rolling texture, Computational Materials Science 47(2) (2009) 448-455.
[28] T. Mayama, M. Noda, R. Chiba, M. Kuroda, Crystal plasticity analysis of texture development in magnesium alloy during extrusion, International Journal of Plasticity 27(12) (2011) 1916-1935.
[29] T. Mayama, T. Ohashi, K. Higashida, Y. Kawamura, Crystal plasticity analysis on compressive loading of magnesium with suppression of twinning, Magnesium Technology, 2011, pp. 273-277.
[30] A. Staroselsky, L. Anand, A constitutive model for hcp materials deforming by slip and twinning: application to magnesium alloy AZ31B, International Journal of Plasticity 19(10) (2003) 1843-1864.
[31] A. Fernandez, M.T.P. Prado, Y.J. Wei, A. Jerusalem, Continuum modeling of the response of a Mg alloy AZ31 rolled sheet during uniaxial deformation, International Journal of Plasticity 27(11) (2011) 1739-1757.
[32] S.R. Agnew, M.H. Yoo, C.N. Tome, Application of texture simulation to understanding mechanical behavior of Mg and solid solution alloys containing Li or Y, Acta Materialia 49(20) (2001) 4277-4289.
[33] R.A. Lebensohn, C.N. Tome, A Self-Consistent Anisotropic Approach for the Simulation of Plastic-Deformation and Texture Development of Polycrystals - Application to Zirconium Alloys, Acta Metallurgica Et Materialia 41(9) (1993) 2611-2624.
[34] S.R. Agnew, O. Duygulu, Plastic anisotropy and the role of non-basal slip in magnesium alloy AZ31B, International Journal of Plasticity 21(6) (2005) 1161-1193.
[35] B. Clausen, C.N. Tome, D.W. Brown, S.R. Agnew, Reorientation and stress relaxation due to twinning: Modeling and experimental characterization for Mg, Acta Materialia 56(11) (2008) 2456-2468.
[36] C.J. Neil, J.A. Wollmershauser, B. Clausen, C.N. Tomé, S.R. Agnew, Modeling lattice strain evolution at finite strains and experimental verification for copper and stainless steel using in situ neutron diffraction, International Journal of Plasticity 26(12) (2010) 1772-1791.
[37] H. Wang, P.D. Wu, J. Wang, Modeling inelastic behavior of magnesium alloys during cyclic loading-unloading, International Journal of Plasticity 47 (2013) 49-64.
[38] C.F. Gu, L.S. Toth, M. Hoffman, Twinning effects in a polycrystalline magnesium alloy under cyclic deformation, Acta Materialia 62 (2014) 212-224.
[39] S.K. Sahoo, L.S. Toth, S. Biswas, An analytical model to predict strain-hardening behaviour and twin volume fraction in a profoundly twinning magnesium alloy, International Journal of Plasticity 119 (2019) 273-290.
[40] C.H. Caceres, P. Lukac, A. Blake, Strain hardening due to {10 12} twinning in pure magnesium, Philosophical Magazine 88(7) (2008) 991-1003.
[41] U.F. Kocks, Laws for work-hardening and low-temperature creep, Journal of Engineering Materials and Technology-Transactions of the ASME 98(1) (1976) 76-85.
[42] H. Mecking, Description of hardening curves of fcc single- and polycrystals, in: A.W. Thompson (Ed.), Work hardening in tension and fatigue: proceedings of a symposium, Cincinnati, Ohio, November 11, 1975. The Metallurgical Society of AIME1977, pp. 67-90.
[43] Y. Estrin, H. Mecking, A unified phenomenological description of work hardening and creep based on one-parameter models, Acta Metallurgica 32(1) (1984) 57-70.
[44] U.F. Kocks, H. Mecking, Physics and phenomenology of strain hardening: the FCC case, Progress in Materials Science 48(3) (2003) 171-273.
[45] M. Gong, G. Liu, J. Wang, L. Capolungo, C.N. Tomé, Atomistic simulations of interaction between basal <a> dislocations and three-dimensional twins in magnesium, Acta Materialia 155 (2018) 187-198.
[46] Y.T. Zhu, X.L. Wu, X.Z. Liao, J. Narayan, L.J. Kecskés, S.N. Mathaudhu, Dislocation-twin interactions in nanocrystalline fcc metals, Acta Materialia 59(2) (2011) 812-821.

[47] S. Ni, Y.B. Wang, X.Z. Liao, R.B. Figueiredo, H.Q. Li, S.P. Ringer, T.G. Langdon, Y.T. Zhu, The effect of dislocation density on the interactions between dislocations and twin boundaries in nanocrystalline materials, Acta Materialia 60(6) (2012) 3181-3189.
[48] Y.F. Shen, L. Lu, Q.H. Lu, Z.H. Jin, K. Lu, Tensile properties of copper with nano-scale twins, Scripta Materialia 52(10) (2005) 989-994.
[49] A. Serra, D.J. Bacon, Interaction of a moving $\{10\bar{1}2\}$ twin boundary with perfect dislocations and loops in a hcp metal, Philosophical Magazine 90(7-8) (2010) 845-861.
[50] A. Serra, D.J. Bacon, Computer simulation of twin boundaries in the h.c.p. metals, Philosophical Magazine A 54(6) (2006) 793-804.
[51] M. Niewczas, Chapter 75 Dislocations and twinning in Face Centred Cubic Crystals, in: F.R.N. Nabarro, J.P. Hirth (Eds.), Dislocations in Solids, Elsevier2007, pp. 263-364.
[52] H. El Kadiri, A.L. Oppedal, A crystal plasticity theory for latent hardening by glide twinning through dislocation transmutation and twin accommodation effects, Journal of the Mechanics and Physics of Solids 58(4) (2010) 613-624.
[53] A.L. Oppedal, H. El Kadiri, C.N. Tome, G.C. Kaschner, S.C. Vogel, J.C. Baird, M.F. Horstemeyer, Effect of dislocation transmutation on modeling hardening mechanisms by twinning in magnesium, International Journal of Plasticity 30-31 (2012) 41-61.
[54] K.D. Molodov, T. Al-Samman, D.A. Molodov, Profuse slip transmission across twin boundaries in magnesium, Acta Materialia 124 (2017) 397-409.
[55] P. Müllner, C. Solenthaler, On the effect of deformation twinning on defect densities, Materials Science and Engineering: A 230(1) (1997) 107-115.
[56] F. Zhang, X. Feng, Z. Yang, J. Kang, T. Wang, Dislocation–twin boundary interactions induced nanocrystalline via SPD processing in bulk metals, Scientific Reports 5 (2015) 8981.
[57] H. Mughrabi, The α-factor in the Taylor flow-stress law in monotonic, cyclic and quasi-stationary deformations: Dependence on slip mode, dislocation arrangement and density, Current Opinion in Solid State and Materials Science 20(6) (2016) 411-420.
[58] A. Vinogradov, Y. Estrin, Analytical and numerical approaches to modelling severe plastic deformation, Progress in Materials Science 95 (2018) 172-242.
[59] S. Allain, J.P. Chateau, O. Bouaziz, A physical model of the twinning-induced plasticity effect in a high manganese austenitic steel, Materials Science and Engineering: A 387–389(0) (2004) 143-147.
[60] R.L. Fullman, Measurement of particle sizes in opaque bodies, Transactions of AIME 197 (1953) 447-452.
[61] J. Gil Sevillano, Geometrically necessary twins and their associated size effects, Scripta Materialia 59(2) (2008) 135-138.
[62] I.J. Beyerlein, L. Capolungo, P.E. Marshall, R.J. McCabe, C.N. Tome, Statistical analyses of deformation twinning in magnesium, Philosophical Magazine 90(16) (2010) 2161-2190.
[63] M. Seleznev, A. Vinogradov, Note: High-speed optical imaging powered by acoustic emission triggering, Review of Scientific Instruments 85(7) (2014) 076103.
[64] A. Ghaderi, M.R. Barnett, Sensitivity of deformation twinning to grain size in titanium and magnesium, Acta Materialia 59(20) (2011) 7824-7839.
[65] L. Capolungo, P.E. Marshall, R.J. McCabe, I.J. Beyerlein, C.N. Tomé, Nucleation and growth of twins in Zr: A statistical study, Acta Materialia 57(20) (2009) 6047-6056.
[66] J. Friedel, Dislocations, 1st English ed., Pergamon Press; Oxford, New York, 1964.
[67] T.E. Mitchell, J.P. Hirth, The shape, configuration and stress field of twins and martensite plates, Acta Metallurgica et Materialia 39(7) (1991) 1711-1717.
[68] L.S. Toth, S. Biswas, C. Gu, B. Beausir, Notes on representing grain size distributions obtained by electron backscatter diffraction, Materials Characterization 84 (2013) 67-71.
[69] M. Fátima Vaz, M.A. Fortes, Grain size distribution: The lognormal and the gamma distribution functions, Scripta Metallurgica 22(1) (1988) 35-40.
[70] R.B. Bergmann, A. Bill, On the origin of logarithmic-normal distributions: An analytical derivation, and its application to nucleation and growth processes, Journal of Crystal Growth 310(13) (2008) 3135-3138.

[71] V. Shterner, A. Molotnikov, I. Timokhina, Y. Estrin, H. Beladi, A constitutive model of the deformation behaviour of twinning induced plasticity (TWIP) steel at different temperatures, Materials Science and Engineering: A 613 (2014) 224-231.
[72] J. Čapek, K. Máthis, B. Clausen, M. Barnett, Dependence of twinned volume fraction on loading mode and Schmid factor in randomly textured magnesium, Acta Materialia 130 (2017) 319-328.
[73] M.R. Barnett, A rationale for the strong dependence of mechanical twinning on grain size, Scripta Materialia 59(7) (2008) 696-698.
[74] Y. Pei, A. Godfrey, J. Jiang, Y.B. Zhang, W. Liu, Q. Liu, Extension twin variant selection during uniaxial compression of a magnesium alloy, Materials Science and Engineering: A 550 (2012) 138-145.
[75] M.A. Kumar, I.J. Beyerlein, C.N. Tomé, Grain size constraints on twin expansion in hexagonal close packed crystals, Journal of Applied Physics 120(15) (2016) 155105.
[76] P.D. Wu, X.Q. Guo, H. Qiao, D.J. Lloyd, A constitutive model of twin nucleation, propagation and growth in magnesium crystals, Materials Science and Engineering: A 625 (2015) 140-145.
[77] V. Livescu, I.J. Beyerlein, C.A. Bronkhorst, O.F. Dippo, B.G. Ndefru, L. Capolungo, H.M. Mourad, Microstructure insensitive twinning: A statistical analysis of incipient twins in high-purity titanium, Materialia 6 (2019) 100303.
[78] C. Lou, X. Zhang, G. Duan, J. Tu, Q. Liu, Characteristics of Twin Lamellar Structure in Magnesium Alloy during Room Temperature Dynamic Plastic Deformation, Journal of Materials Science & Technology 30(1) (2014) 41-46.
[79] K. Radhakrishnan, A.C. Hindmarsh, Description and Use of LSODE, the Livermore Solver for Ordinary Differential Equations, NASA Reference Publication 1327, Lawrence Livermore National Laboratory Report UCRL-ID-113855 NASA, Cleveland, OH, USA, 1993, pp. 1-108.
[80] L. Lasdon, A. Duarte, F. Glover, M. Laguna, R. Martí, Adaptive memory programming for constrained global optimization, Computers & Operations Research 37(8) (2010) 1500-1509.
[81] R. Storn, K. Price, Differential Evolution – A Simple and Efficient Heuristic for global Optimization over Continuous Spaces, Journal of Global Optimization, 11(4) (1997) 341-359.
[82] K. Máthis, G. Csiszár, J. Čapek, J. Gubicza, B. Clausen, P. Lukáš, A. Vinogradov, S.R. Agnew, Effect of the loading mode on the evolution of the deformation mechanisms in randomly textured magnesium polycrystals – Comparison of experimental and modeling results, International Journal of Plasticity 72 (2015) 127-150.
[83] E. Pomponi, A. Vinogradov, A real-time approach to acoustic emission clustering, Mechanical System and Signal Processing 40(2) (2013) 791-804.
[84] A. Vinogradov, D. Orlov, A. Danyuk, Y. Estrin, Effect of grain size on the mechanisms of plastic deformation in wrought Mg–Zn–Zr alloy revealed by acoustic emission measurements, Acta Materialia 61(6) (2013) 2044-2056.
[85] A. Vinogradov, A. Lazarev, M. Linderov, A. Weidner, H. Biermann, Kinetics of deformation processes in high-alloyed cast transformation-induced plasticity/twinning-induced plasticity steels determined by acoustic emission and scanning electron microscopy: Influence of austenite stability on deformation mechanisms, Acta Materialia 61(7) (2013) 2434-2449.
[86] D. Orlov, G. Raab, T.T. Lamark, M. Popov, Y. Estrin, Improvement of mechanical properties of magnesium alloy ZK60 by integrated extrusion and equal channel angular pressing, Acta Materialia 59(1) (2011) 375-385.
[87] C.A. Schneider, W.S. Rasband, K.W. Eliceiri, NIH Image to ImageJ: 25 years of image analysis, Nature Methods 9 (2012) 671.
[88] J. Čapek, K. Máthis, B. Clausen, J. Stráská, P. Beran, P. Lukáš, Study of the loading mode dependence of the twinning in random textured cast magnesium by acoustic emission and neutron diffraction methods, Materials Science and Engineering: A 602 (2014) 25-32.
[89] D. Drozdenko, J. Čapek, B. Clausen, A. Vinogradov, K. Máthis, Influence of the solute concentration on the anelasticity in Mg-Al alloys: A multiple-approach study, Journal of Alloys and Compounds 786 (2019) 779-790.
[90] A. Vinogradov, E. Vasilev, M. Seleznev, K. Máthis, D. Orlov, D. Merson, On the limits of acoustic emission detectability for twinning, Materials Letters 183 (2016) 417-419.
[91] A. Vinogradov, E. Vasilev, M. Linderov, D. Merson, Evolution of Mechanical Twinning during Cyclic Deformation of Mg-Zn-Ca Alloys, Metals 6(12) (2016) 304.

[92] L. Jiang, J.J. Jonas, R.K. Mishra, A.A. Luo, A.K. Sachdev, S. Godet, Twinning and texture development in two Mg alloys subjected to loading along three different strain paths, Acta Materialia 55(11) (2007) 3899-3910.
[93] D.W. Brown, S.R. Agnew, S.P. Abeln, W.R. Blumenthal, M.A.M. Bourke, M.C. Mataya, C.N. Tomé, S.C. Vogel, The role of texture, temperature, and strain rate in the activity of deformation twinning, 2005, pp. 1037-1042.

Figures

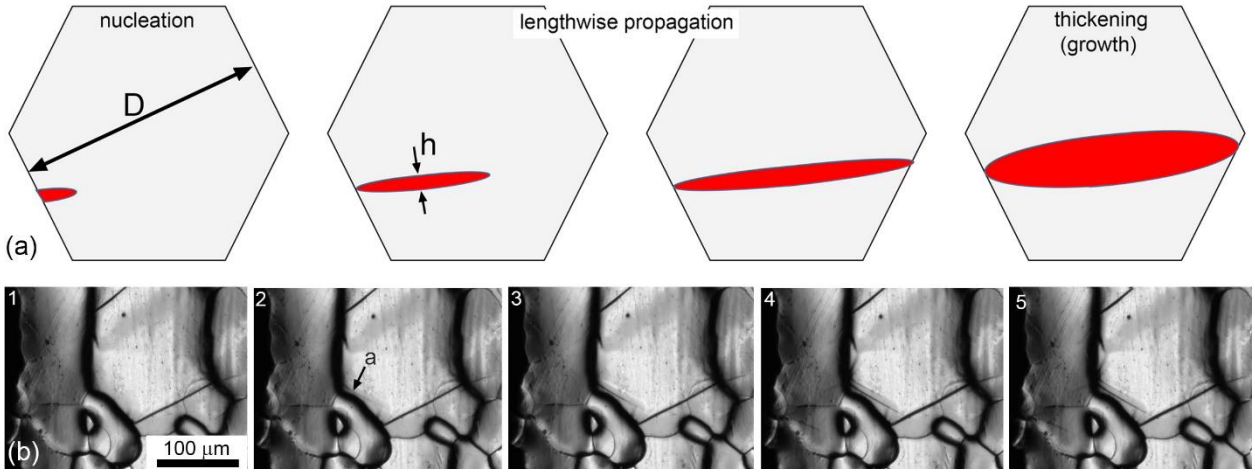

Figure 1. Schematics of twin nucleation, propagation and growth (a) and direct video observation (b) illustrating this process in pure Mg under compression at the strain rate $\dot{\varepsilon} = 1\times10^{-3}$ s^{-1}; the arrow labeled "a" on the second snapshot points to a freshly emerged twin. The successive snapshots were taken at a rate of 50 fps. (The experimental setup is described in [62].)

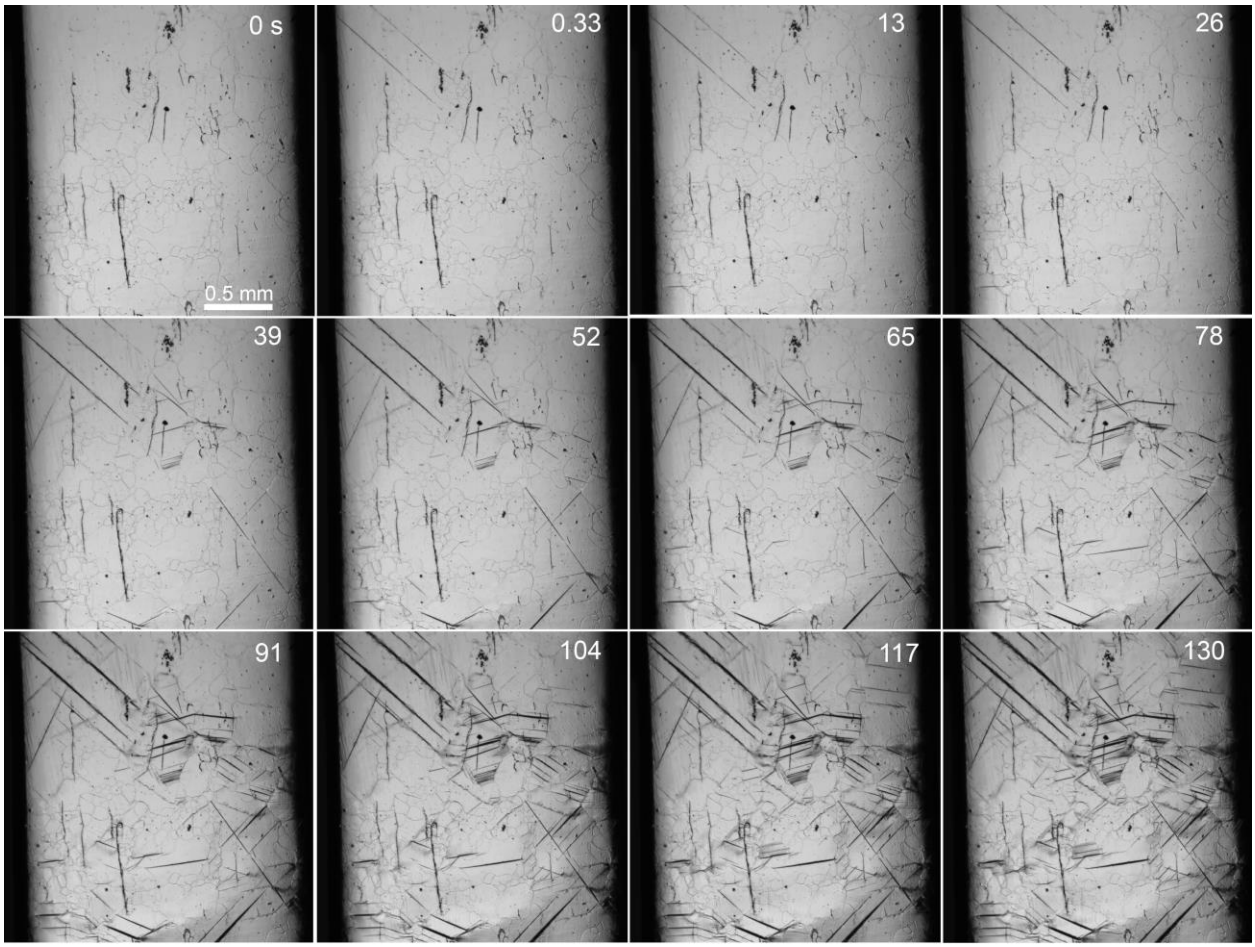

Fig. 2. Sequence of frames from a video record of deformation twinning in as-cast polycrystalline magnesium under uniaxial compression at a strain rate of $\dot{\varepsilon}$ = 5×10^{-3} s^{-1}; the first "reference" frame was taken at the total strain of 2×10^{-4} ; the time (in seconds) is indicated in the upper right corner of each frame.

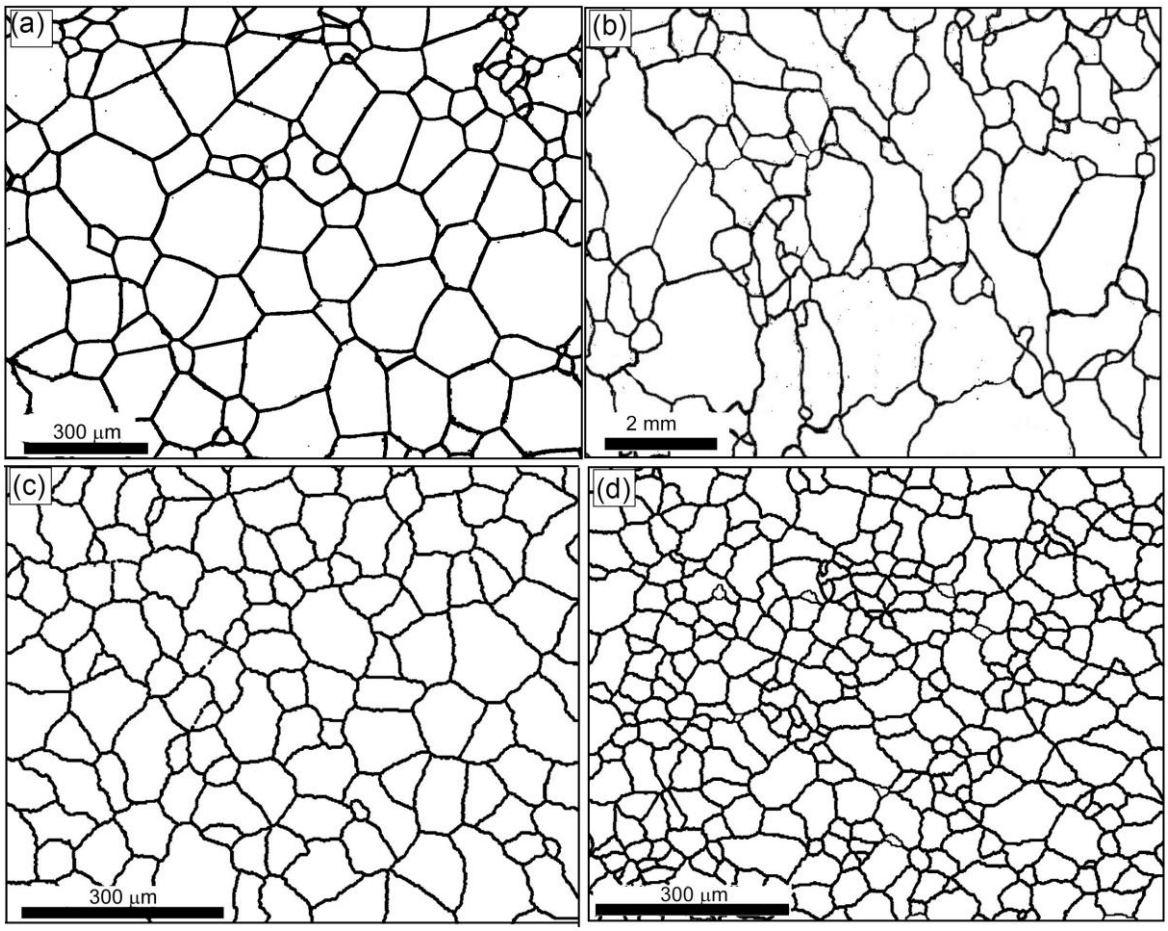

Figure 3. Examples of binarised microscopic images used to evaluate the grain size distributions in pure Mg and Mg alloy ZK60: (a) as-cast Mg with comparatively small grain size, (b) as-cast Mg with coarse grains and a large variance of grain shapes and dimensions, (c) hot-extruded Mg, and (d) hot-pressed ZK60.

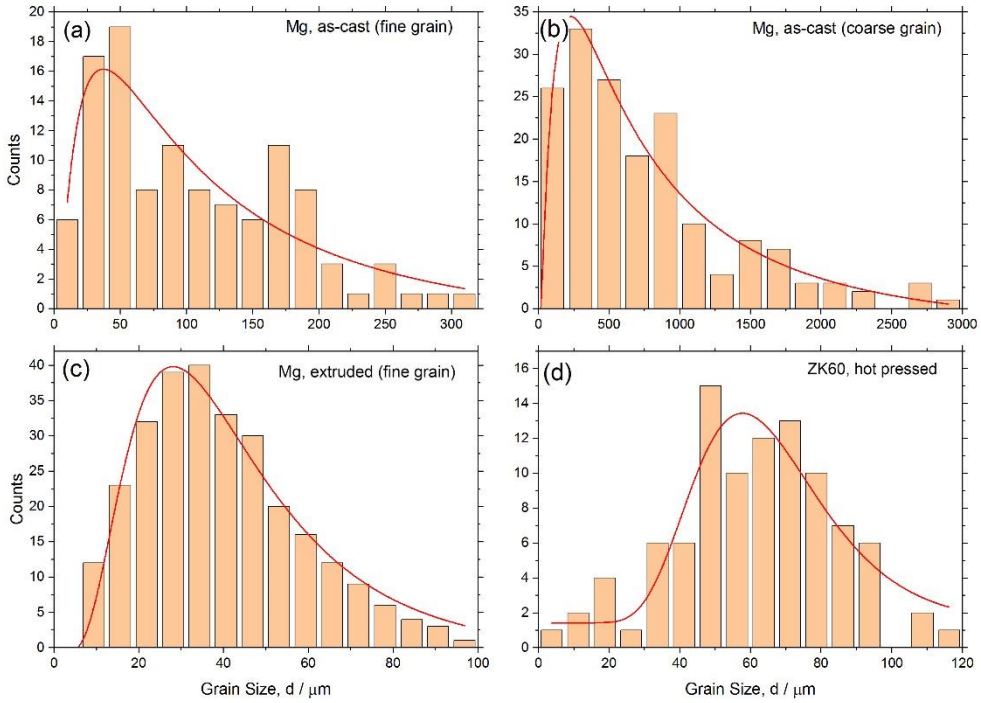

Figure 4. Grain size (the area-based effective diameter) distributions for examples shown in Fig. 1: (a) as-cast Mg with relatively small grain size (b) as-cast Mg with coarse grains and a large variance of grain shapes and dimensions, (c) hot-extruded Mg, and d) hot-pressed ZK60. (The ImageJ software was used to obtain these distributions from binarised maps.)

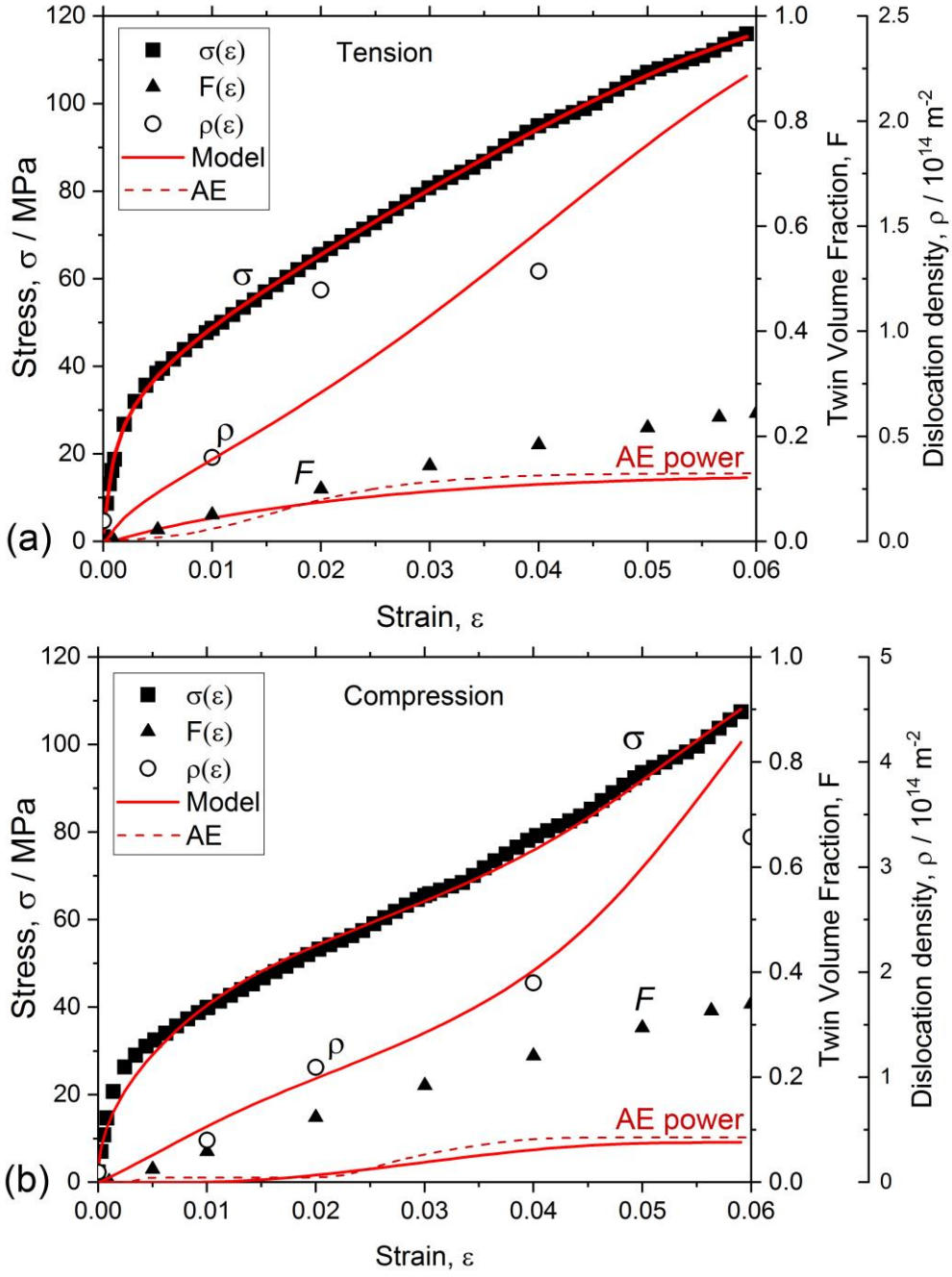

Figure 5. Stress-strain curves for *in situ* tension (a) and compression (b) testing of the as-cast polycrystalline Mg samples (corresponding to case (a) in Figs. 3 and 4) and their approximation by model results. Measured (symbols) and predicted (solid lines) total dislocation density and twin volume fraction are shown for comparison. The dashed lines represent the cumulative AE power normalised to unity obtained for the AE cluster associated with twinning.

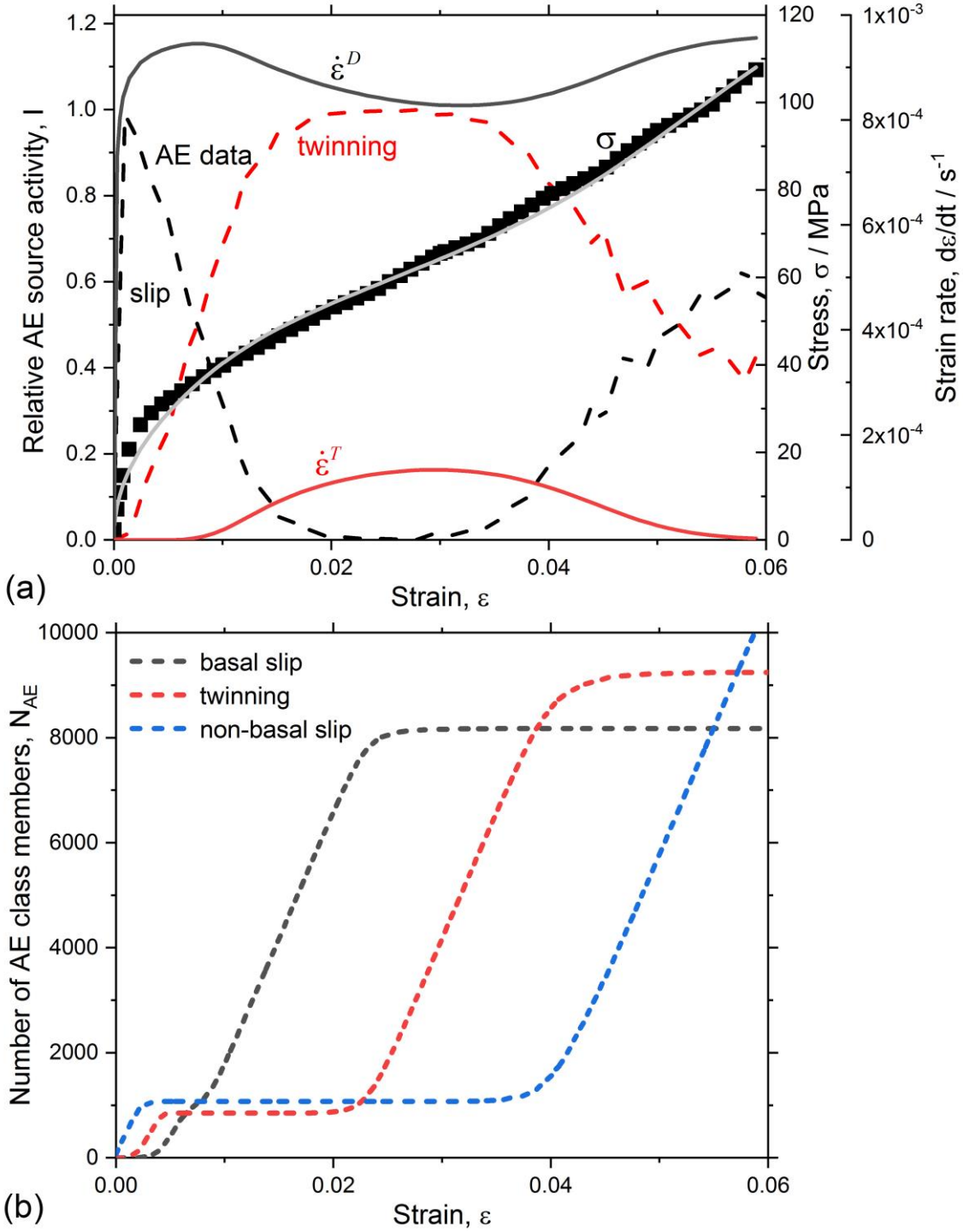

Figure 6. Results of the modelling of the stress-strain behaviour during *in situ* compression testing of the as-cast polycrystalline Mg sample (same as in Fig.5) and the calculated plastic strain rates accommodated by the principal deformation modes: dislocation slip and twinning. The *in situ* AE results characterising the activity of both mechanisms are plotted alongside the predicted evolution of $\dot{\varepsilon}^D$ and $\dot{\varepsilon}^T$ for comparison.

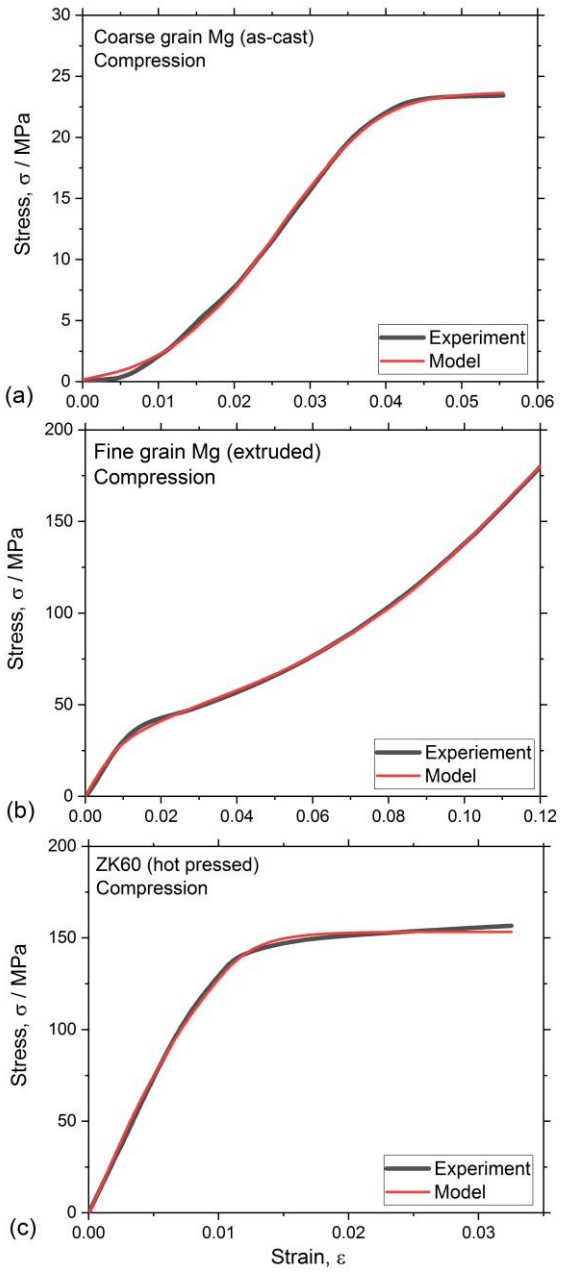

Figure 7. A comparison between the calculated and the experimental stress-strain curves for pure Mg with different grain size distributions and Mg alloy ZK60 deformed in compression at room temperature. The labelling of the sub-figures (a-c) corresponds to that in Figs. 3 (b-d) and 4 (b-d).

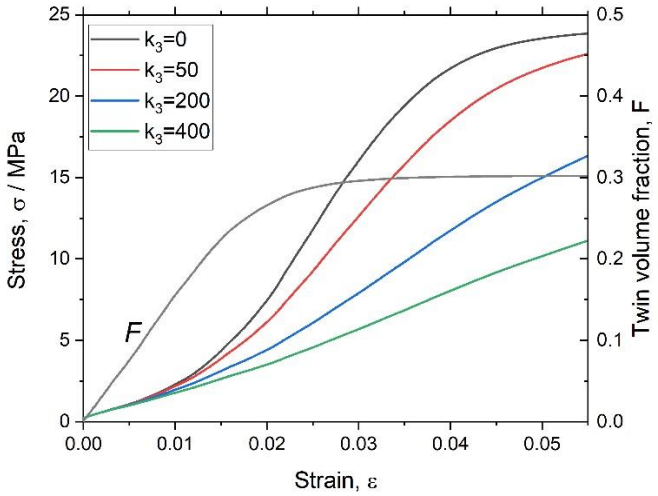

Figure 8. A family of calculated stress-strain curves illustrating the effect of the dislocation annihilation due to the twin-dislocation interaction (In these calculations, k_3 in Eq. (7) was varied while all other parameters of the model were kept constant.)